Journal of The Electrochemical Society, **164** (14) A3454-A3461 (2017)
0013-4651/2017/164(14)/A3454/8/$37.00 © The Electrochemical Society

A Strategy to Make High Voltage $LiCoO_2$ Compatible with Polyethylene Oxide Electrolyte in All-Solid-State Lithium Ion Batteries

Jun Ma,[a] Zhaolin Liu,[a] Bingbing Chen,[a] Longlong Wang,[a,b] Liping Yue,[a] Haisheng Liu,[a] Jianjun Zhang,[a,b] Zhihong Liu,[a] and Guanglei Cui[a,z]

[a]*Qingdao Industrial Energy Storage Research Institute, Qingdao Institute of Bioenergy and Bioprocess Technology, Chinese Academy of Sciences, Qingdao 266101, People's Republic of China*
[b]*University of Chinese Academy of Sciences, Beijing 100049, People's Republic of China*

Interface stability between cathode and electrolyte is closely related to the interface resistance and electrochemical performance of all-solid-state lithium ion batteries (LIBs). However, the significant interface issues between cathode and all-solid-state polymer electrolyte have been researched rarely. Here, we demonstrate that severe interface decomposition reactions occur continually and deteriorate the cycling life of high voltage $LiCoO_2$/cellulose-supported poly(ethylene oxide) (PEO)-lithium difluoro(oxalato)borate (LiDFOB)/Li battery between 2.5 and 4.45 V vs. Li/Li^+. To improve the interface stability between $LiCoO_2$ and PEO-LiDFOB electrolyte, we modify the $LiCoO_2$ surface by a thin layer of high ionic conducting and electrochemical oxidation resistant poly(ethyl cyanoacrylate) (PECA) through in-situ polymerization method. The PECA coating layer significantly suppresses the continuous decomposition of lithium difluoro(oxalato)borate (LiDFOB) salt in PEO electrolyte. As a result, the PECA-coated $LiCoO_2$/PEO-LiDFOB/Li battery shows decreased interface resistance and enhanced cycling stability. This work will enlighten the understanding of interface stability and enrich the modification strategy between cathode and polymer electrolyte as well as boost the further development of all-solid-state LIBs.

Manuscript submitted September 8, 2017; revised manuscript received October 30, 2017. Published November 11, 2017.

Polymer electrolyte-based all-solid-state lithium ion batteries (LIBs) with the merits of flexibility, high energy density and high safety have been researched for a long time.[1–5] Nevertheless, their applications are still challenged by the interface issues between electrode and solid-state electrolyte. The thorny interface issues mainly refer to the inherent space charge layer and detrimental chemical reactions at the electrode and electrolyte interface, which lead to large interface impedance and then deteriorate the fast charging/discharging ability and cycling stability of all-solid-state LIBs.[6–9]

Polyethylene oxide (PEO) electrolyte with high ion conductivity and good interface stability with Li metal has been successfully used in commercial polymer LIBs, in which the cathode material is $LiFePO_4$ instead of $LiCoO_2$. The failure application of PEO electrolyte in $LiCoO_2$-based high energy density LIBs is mainly due to the interface decomposition reactions of PEO at high voltage. Shiro Seki et al. have proposed that the oxidation decomposition of PEO electrolyte takes place from 4.0 V vs. Li/Li^+, which leads to continuous increasing of $LiCoO_2$/PEO interfacial resistance and results in poor cycle performance at 4.4 V vs. Li/Li^+.[10] Moreover, during high voltage charging of $LiCoO_2$, the highly oxidized Co^{4+} ions will accelerate the oxidation decomposition of PEO electrolyte.[11] It can be concluded that the cathode/polymer electrolyte interface characteristic is quite essential to the electrochemical performance of all-solid-state LIBs, especially for the high voltage cathode $LiCoO_2$ and PEO electrolyte. However, the interface oxidation decomposition products and reaction mechanism between $LiCoO_2$ and PEO electrolyte have not been studied clearly. Thus, there is still much work to do to understand and optimize the interface stability between the widely used cathode material $LiCoO_2$ and PEO electrolyte for high voltage (exceeding 4.4 V vs. Li/Li^+) applications.

Surface coating of $LiCoO_2$ powder is a powerful strategy to enhance the interface stability with PEO electrolyte at high working potential. Generally, moderate amount of polymer electrolyte is added into the electrode to guarantee the three dimensional Li^+ ion conductive pathways in polymer electrolyte-based all-solid-state LIBs. As a result, the $LiCoO_2$ active material contacts with PEO electrolyte not only on the cathode/electrolyte interface but also in the cathode itself. Some inorganic coating materials, such as $Li_{1.5}Al_{0.5}Ge_{1.5}(PO_4)_3$, Li_3PO_4, and Al_2O_3, acting as an oxidation barrier for PEO electrolyte, have displayed significant improvement to the $LiCoO_2$/PEO interface at high voltage above 4.4 V vs. Li/Li^+.[10–13] But, element interdiffusion at the inorganic coating materials and $LiCoO_2$ interface is usually inevitable during high temperature sintering process. Moreover, the reported inorganic coating materials are feeble to remarkably improve the cycling stability of $LiCoO_2$/PEO/Li all-solid-state batteries. To overcome the above problems, the simple and low-temperature polymer coating seems to be a wise choice. Our group has demonstrated that the uniform and conformal poly(ethyl α-cyanoacrylate) (PECA) polymer coating layer on the surface of 5 V cathode $LiNi_{0.5}Mn_{1.5}O_4$ can be prepared by in-situ polymerization of ethyl α-cyanoacrylate (ECA) monomers in air at room temperature.[14] Interestingly, the strong electron withdrawing group of -C≡N in PECA makes the coating layer have excellent properties, including high voltage window (5 V vs. Li/Li^+), fast Li ion transport, blocking transition metallic ions, buffering electrolyte corrosion and particle cracks, et al. As a result, the PECA-coated $LiNi_{0.5}Mn_{1.5}O_4$ possesses significantly enhanced cycling stability in commercial liquid electrolyte. Therefore, the PECA coating layer with the strong electron withdrawing group of -C≡N and high voltage window is expected to suppress the oxidation decomposition of PEO electrolyte when it directly contacts with the high voltage $LiCoO_2$.

Here, we investigated the interface reaction and proposed a simple and effective strategy to enhance the interface stability between high voltage $LiCoO_2$ (4.45 V vs. Li/Li^+) and solid PEO electrolyte by introducing the PECA buffer layer. We successfully constructed the PECA buffer layer on the $LiCoO_2$/PEO interface through a simple and low-temperature polymer coating method. The electrochemical performance of $LiCoO_2$/PEO/Li batteries before and after PECA modification was evaluated carefully. Furthermore, the modification mechanism of PECA buffer layer was proposed based on the comprehensive ex-situ measurements and density function theory (DFT) calculation results.

Experimental

Preparation of PEO electrolyte.—The rigid-flexible coupling cellulose-supported PEO solid-state electrolyte was synthesized by a method reported by our previous work.[15] PEO (Mw = 300,000, Alfa Aesar Company), lithium difluoro(oxalato)borate (LiDFOB, Jiangsu Guotai Super Power New Materials Co., Ltd.), succinonitrile (SN, Aladdin Company), and acetonitrile (AN, Macklin Company) (10:1:9:120 by weight) were mixed and stirred in a sealed bottle for

[z]E-mail: cuigl@qibebt.ac.cn

12 hours. Then, the liquid PEO electrolyte was casted onto both sides of cellulose membrane (Nippon Kodoshi Corporation) with doctor-blade and dried at 50°C for 12 hours. The obtained electrolyte was denoted as PEO-LiDFOB in the following text.

Preparation of PECA-coated $LiCoO_2$.—First, ethyl cyanoacrylate (ECA, Sinopharm Chemical Reagent Co., Ltd.) was dissolved in acetone (AE, Sinopharm Chemical Reagent Co., Ltd.) solvent in a sealed vial with an inert atmosphere and stirred evenly. The weight ratio of ECA:AE is 1:3. Next, 2.0 g commercial $LiCoO_2$ (Contemporary Amperex Technology Co., Ltd.) powder was mixed with 0.163 g (2 wt%, relative to $LiCoO_2$) as-prepared solution and 6.0 g acetone and stirred vigorously under an Argon gas for 3 hours. Then the mixed solution was concentrated by rotary evaporation. Finally, the obtained PECA-coated $LiCoO_2$ powder was dried in a vacuum oven at 60°C for 3 hours to remove the residual acetone solvent completely.

Characterizations.—The X-ray diffraction (XRD) patterns of $LiCoO_2$ powders before and after PECA coating were obtained by using a Bruker-AXS Micro diffractometer (D8 Advance) with Cu-Kα radiation ($\lambda = 1.5406$ Å) from 10° to 80°. Transmission and reflection Fourier transform infrared spectroscopy (FTIR) spectra were carried out using EO-SXB IR spectrometer in the wavenumber range of 400–4000 cm^{-1} and 700–4000 cm^{-1}, respectively. Raman spectra were recorded by a Thermo Scientific DXRxi system with excitation from an Ar laser at 532 nm at ambient temperature. X-ray photoelectron spectroscopy (XPS) was obtained by using a focused monochromatized Al Kα radiation (1486.6 eV). C1s (284.8 eV) of contaminated carbon in the vacuum chamber was used to calibrate the binding energy. Energy dispersive X-ray spectrometer (EDS) was collected on a HITACHI S-4800 at an accelerating voltage of 15 kV. Scanning electron microscope (SEM) and transmission electron microscope (TEM) images were performed with field emission scanning electron microscopy (FESEM, HITACHI S-4800) and transmission electron microscopy (TEM, JEOL 2010F), respectively.

Electrochemical measurements.—To prepare $LiCoO_2$ cathode, the $LiCoO_2$ or PECA-coated $LiCoO_2$ powder, acetylene black (TIMCAL Ltd.), poly(vinylidene fluoride)-anhydride (PVDF-AD, Solvay Company), and PEO solution were added to a mortar at a ratio of 85:5:7:3 in weight and grinded for 1.5 hours with suitable N-methyl-2-pyrrolidone (NMP, Aladdin Company). Notably, the PEO solution was prepared by mixing and stirring the PEO (Mw = 300,000), LiDFOB, SN, and NMP (10:1:9:90 by weight) in a sealed bottle for 6 hours at 60°C. Then, the mixed slurry was coated onto an aluminum foil (Sigma-Aldrich Co. LLC) with a doctor-blade. After drying, the $LiCoO_2$ cathode sheet was punched out in diameter (14 mm) pieces with the active material mass loading about 2.15 mg/cm^2 and then dried in vacuum oven at 120°C for 24 hours. All-solid-state polymer batteries were assembled in an argon-filled glove box by utilizing as-prepared cathode, solid-state electrolyte membrane and Li foil (China Energy Lithium Co., Ltd.). The galvanostatic discharge-charge performance of cells were tested on a LAND battery test system in 80°C oven at 0.1 C (1C = 160 mAh/g) between 2.5 V and 4.45 V vs. Li/Li^+.

Electrochemical impedance spectroscopy (EIS) studies were carried out by applying a sine wave with an amplitude of 5.0 mV over the frequency range from 0.1 Hz to 4×10^6 Hz on the Zahner Zennium electrochemical working station. The code Zview was used to fit the impedance spectra to the proposed equivalent circuit. The linear sweep voltammetry experiment of Li/PEO-LiDFOB/stainless steel (SS) coin cell was conducted at a scan rate of 1.0 mV/s from the open circuit voltage (OCV) to 6.0 V vs. Li/Li^+ at 80°C in order to test the stable electrochemical window of PEO-LiDFOB electrolyte. The ionic conductivity of PEO-LiDFOB electrolyte was measured by alternating current (AC) impedance method. The SS/PEO-LiDFOB/SS coin cell was tested from 30°C to 80°C with an amplitude of 5.0 mV over the frequency range from 0.1 Hz to 4×10^6 Hz on the Zahner Zennium electrochemical working station. According to the formula of $\sigma = L/(R \cdot S)$, where σ (S/cm) was the ionic conductivity, L (cm) was the thickness of electrolyte, R (Ω) was the impedance, and S (cm^2) was the contact area of electrolyte with the electrode, the ionic conductivity of PEO-LiDFOB electrolyte was calculated.

DFT calculations.—The plane-wave based DFT method was implemented in the Vienna ab initio simulation package (VASP), with a standard GGA functional in the framework of Perdew-Burke-Ernzerhof (PBE).[16,17] The surface structure was relaxed with cutoff energy of 550 eV for the plane wave basis set. A $5 \times 5 \times 2$ mesh in the Monkhorst-Pack scheme was sufficient in the energetic relaxation of surface structure.[18,19] Herein, the Hubbard model corrections were used with an effective single U-J parameter of 4.9 eV for the Co-3d state, according to previously reports.[20] In addition, the fully relaxed structure was considered completed when the magnitude of the force on each atom was smaller than 0.05 eV Å and a total energy convergence within 10^{-5} eV per unit cell in all calculation.

Results and Discussion

Preparation of PECA-coated $LiCoO_2$ powder.—Figure 1 compared the structure and morphology of $LiCoO_2$ powders before and after PECA coating by in-situ polymerization method. The XRD results in Figure 1a showed that the crystal structure of $LiCoO_2$ was retained after PECA coating. Both samples had hexagonal crystal structure and belonged to R-3m space group. In addition, no impurities were detected from the PECA-coated $LiCoO_2$. The SEM images in Figures 1b and 1c displayed that the PECA-coated $LiCoO_2$ had the same particle morphology and size with that of $LiCoO_2$. Their corresponding TEM images in Figures 1d–1g indicated an amorphous layer of about 50 nm coated uniformly on the surface of PECA-coated $LiCoO_2$. Furthermore, the mapping results in Figure 1h displayed the uniform distribution of Co and N elements on the surface of PECA-coated $LiCoO_2$, which suggested the successfully uniform coating of PECA on the surface of $LiCoO_2$.

To confirm the composition of PECA layer on the surface of $LiCoO_2$ and whether interaction occurred between PECA and $LiCoO_2$, FTIR, Raman and XPS measurements were conducted. Figures 2a and 2b showed the FTIR and Raman results of $LiCoO_2$, PECA-coated $LiCoO_2$ powders, and PECA, respectively. The FTIR peaks of these samples between 400 and 700 cm^{-1} were attributed to the variations of CoO_6 octahedron, which were consistent with the Raman shifts at 482 cm^{-1} and 595 cm^{-1}.[21] These results suggested the structure of $LiCoO_2$ was not changed after PECA coating. In the FTIR spectrum, the sign of ECA monomers polymerized to PECA was the disappearance of peaks at 3129 and 1615 cm^{-1}, which respectively corresponded to the functional groups of =CH and C=C in ECA monomers.[22,23] Here, compared with the FTIR spectrum of ECA monomer (Figure S1), the peaks appearing at 2998 (CH_2), 1753 (C=O), and 1256 (C-O) cm^{-1} but vanishing at 3129 (=CH) and 1615 (C=C) cm^{-1} in Figure 2a indicated the successful in-situ polymerization of PECA on the surface of $LiCoO_2$ particles.[22,23] However, the polymerization of ECA monomers could reduce the conjugation between C≡N (2238 cm^{-1}), C=C, and C=O groups, resulting in the peak blueshift as well as the decreased peak intensity of C≡N group in the FTIR spectra.[23,24] Furthermore, the small amount (2 wt%) of PECA in $LiCoO_2$ powder made it difficult to detect the C≡N group by FTIR technique. Therefore, we measured Raman spectra and confirmed the existence of C≡N group at 2252 cm^{-1} in PECA-coated $LiCoO_2$ in Figure 2b.[25] The XPS results in Figure 2c further identified the polymerization of PECA on the surface of $LiCoO_2$, as demonstrated by the peaks with binding energies at 286.5 eV (C1s of C-O), 289.0 eV (C1s of C=O-O), 399.6 eV (N1s of C≡N), and 532.4 eV (O1s of C-O and C=O-O).

On the other hand, the interaction between PECA and $LiCoO_2$ is also discussed based on the XPS results (Figure 2c). In general, the strong polar groups of C≡N (399.3 eV, N1s) and C=O-O (533.1 eV, O1s) play an essential role in the strong adhesion properties of PECA.

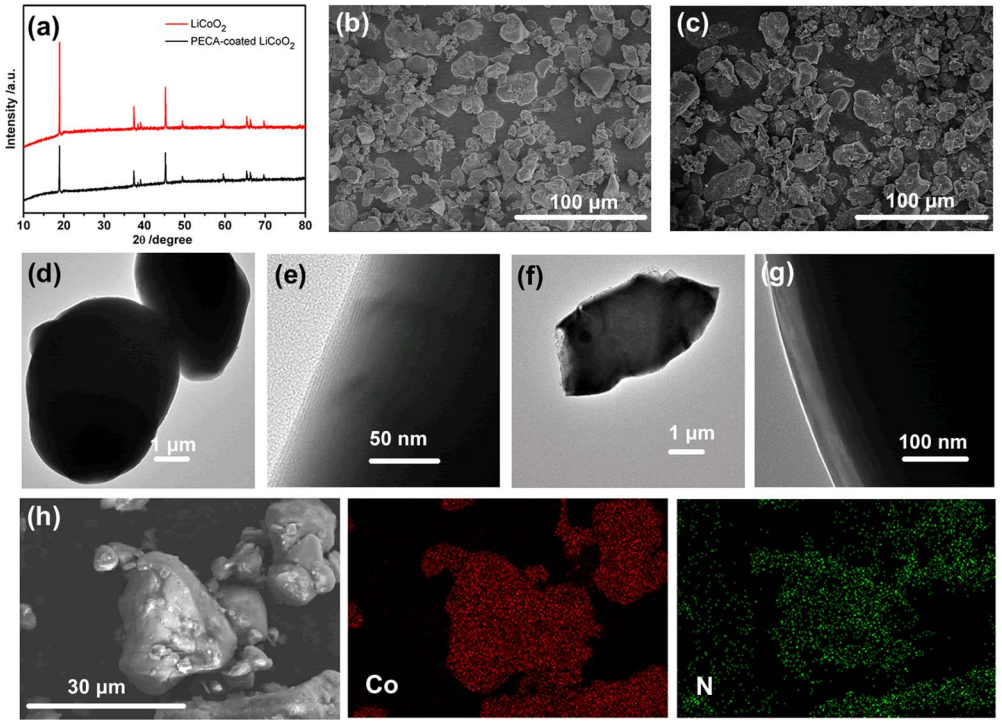

Figure 1. (a) XRD patterns of $LiCoO_2$ and PECA-coated $LiCoO_2$. Typical SEM images of (b) $LiCoO_2$ and (c) PECA-coated $LiCoO_2$. Typical TEM images of (d, e) $LiCoO_2$ and (f, g) PECA-coated $LiCoO_2$. (h) Typical SEM image and the corresponding Co and N element mapping results of PECA-coated $LiCoO_2$.

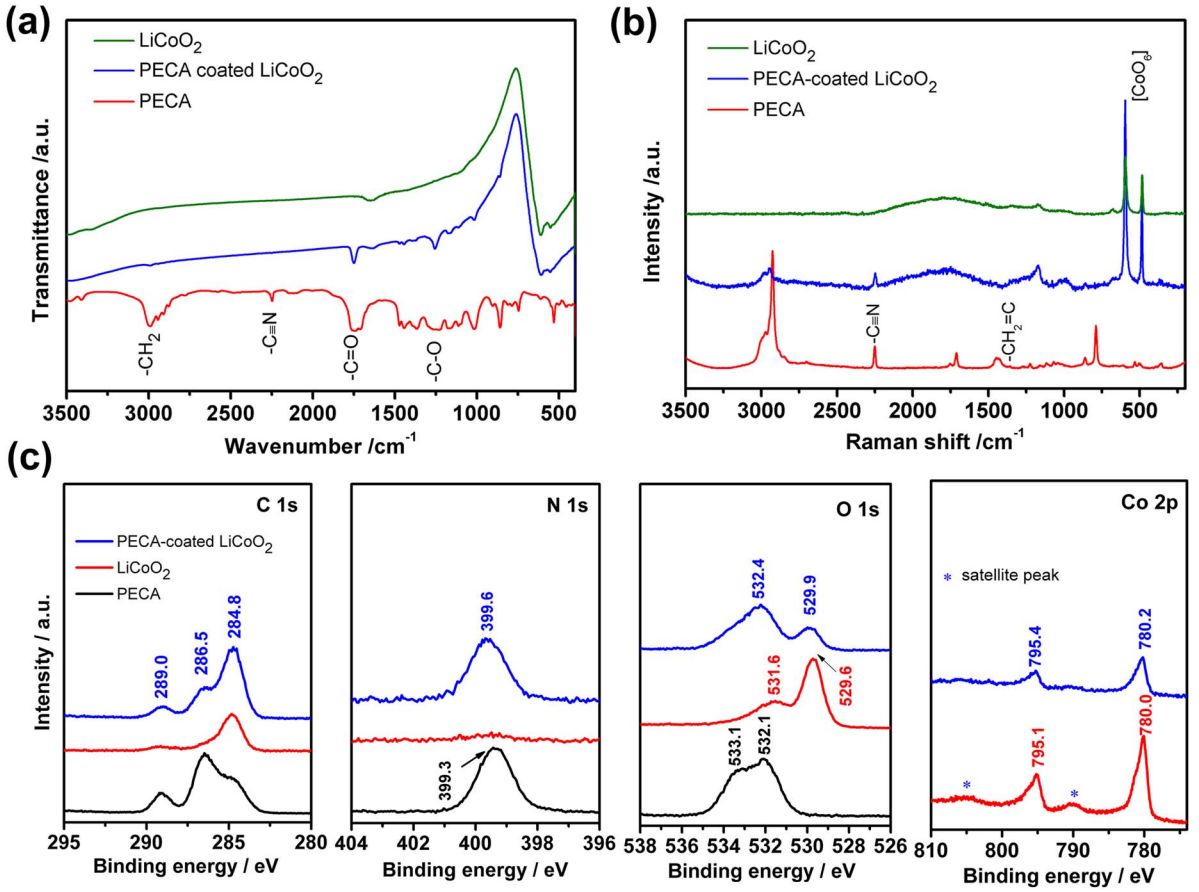

Figure 2. (a) FTIR, (b) Raman, and (c) XPS spectra of $LiCoO_2$, PECA-coated $LiCoO_2$, and PECA.

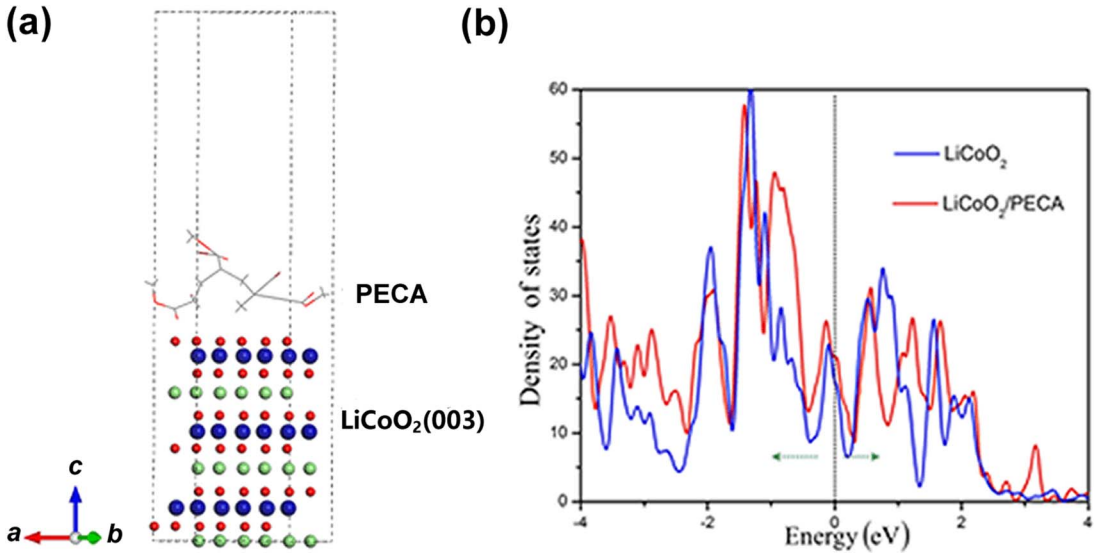

Figure 3. (a) The interface model of $LiCoO_2$ surface and PECA. (b) Total DOS for the interface and surface structure.

After PECA coating on the $LiCoO_2$ particles, the functional group C≡N (399.6 eV, N1s) displayed a little higher binding energy. However, the functional group C=O-O (at about 533.1 eV, O1s) showed remarkably decreased relative intensity. As for $LiCoO_2$, the binding energy of lattice oxygen in $LiCoO_2$ (529.6 eV, O1s) shifted slightly to higher binding energy side in the XPS spectrum of PECA-coated $LiCoO_2$ (529.9 eV, O1s). Furthermore, the Co2p binding energy also increased slightly after PECA coating. The increased O1s and Co2p binding energy of PECA-coated $LiCoO_2$ further confirmed the decreased electron cloud density due to the interaction between lattice O^{2-} or Co^{3+} ions and the electron withdrawing groups of PECA, such as C=O-O and C≡N.[26] In addition, the O1s peak at 531.6 eV indicated the existence of Li_2CO_3, which was usually observed on the surface of layer-structured oxides.[27] Li_2CO_3 remained on the surface of $LiCoO_2$ after PECA coating, as demonstrated by the broad and asymmetric O 1s peak at 532.4 eV.

Due to the above interaction between $LiCoO_2$ and PECA, the PEO electrolyte would not be oxidized easily by $LiCoO_2$ when the electron withdrawing buffer layer PECA was introduced. This conclusion was confirmed by the DFT calculation results (Figure 3). The first principles were employed to understand the reduction stability of PECA layer on the surface of $LiCoO_2$. The relatively stable $LiCoO_2$ (003) surface was investigated to discuss the $LiCoO_2$ coated by PECA modeling with 13 Å thick vacuum layers, which is shown in the Figure S2. Firstly, the projected density of states (PDOS) was discussed for evaluating surface property of $LiCoO_2$ (003). In addition, the corresponding PDOS for bulk $LiCoO_2$ were also shown. From the Figure S3, it was clear that the introduction of a surface affected the electronic structure of the bulk $LiCoO_2$ (bandgap 1.87 eV). These results were in agreement with the previously report.[18] For example, the bandgap between the valance and conduction band would decrease in surface region, and it showed the metallic character. In addition, the exposed Li-O groups would easily react with the PEO electrolyte, which may induce the interface reaction during high voltage charging. Therefore, in our work, we established the interface model with the 2×2 $LiCoO_2$ (003) surface supercell and PECA, as shown in the Figure 3a. A relatively small interface supercell was chosen with a reasonable balance of computation cost. We mainly examined the effect of PECA coating layer on the $LiCoO_2$ surface electronic structure. The total PDOS can be calculated for interface structure (Figure 3b). After coated with PECA, the conduction band part of $LiCoO_2$ shifted toward higher energy obviously, and the valance band part shifted toward lower energy, which decreased the oxidation stability of $LiCoO_2$ surface. These results may indirectly suggest that the $LiCoO_2$ structure coated by PECA would improve the electrochemical stability with the PEO electrolyte.

Preparation and evaluation of PEO-LiDFOB electrolyte.—The cellulose-supported PEO-LiDFOB solid-state electrolyte was prepared by the method reported by our group previously.[15] The morphology, electrochemical window, and ionic conductivity of the obtained cellulose-supported PEO-LiDFOB electrolyte were characterized and displayed in Figure 4. The SEM images showed that the PEO-LiDFOB electrolyte had smooth surface and a thickness of about 30 μm. The PEO electrolyte filled uniformly in the porous structure of cellulose, which formed the three dimensional-connected pathways for Li^+ ions diffusion. The linear sweep voltammetry curve of Li/PEO-LiDFOB/SS coin cell under a scan rate of 1.0 mV/s at 80°C indicated that the stable electrochemical window of PEO-LiDFOB electrolyte was about 4.2 V vs. Li/Li^+. However, when the cutoff voltage was limited at 4.45 V vs. Li/Li^+, almost identical FTIR spectra (Figure S4) of this solid-state polymer electrolyte before and after linear sweep voltammetry measurement was obtained. This may be due to the very little electrolyte decomposition during the linear sweep voltammetry measurement. The ionic conductivity of PEO-LiDFOB electrolyte from 30°C to 80°C was calculated based on the EIS measurement results (Figure S5). The linear temperature dependence of ionic conductivity for PEO-LiDFOB electrolyte was observed in the range of 30–80°C. The ionic conductivity for PEO-LiDFOB electrolyte at 30°C was 1.03×10^{-4} S/cm. When the temperature rose to 80°C, the ionic conductivity increased to 8.95×10^{-4} S/cm, which was similar to the reported PEO-based electrolytes.[3] The interface compatibility between PEO-LiDFOB electrolyte and Li metal anode was also evaluated by the constant current polarization measurement in symmetric Li/PEO-LiDFOB/Li cell at 80°C, as shown in Figure 4e. After charging and discharging sequentially under a constant current of 0.2 mA/cm^2 for 100 hours, the cell voltage remained nearly constant between 0.5 V and −0.5 V vs. Li/Li^+. No short circuit or remarkable polarization was observed. Furthermore, the SEM image of the Li metal anode after the constant current polarization measurement displayed uniform distribution of Li particles without Li dendrite formation. Therefore, the high ionic conductivity and high interface stability with Li metal anode made the prepared PEO-LiDFOB electrolyte competent to the following battery measurement between 2.5 V and 4.45 V vs. Li/Li^+.

Electrochemical measurements.—The commercial $LiCoO_2$ powder as cathode material had stable cycling performance in liquid electrolyte (1M $LiPF_6$ in EC:DMC = 1:1 v/v)) between 2.5 V and 4.45

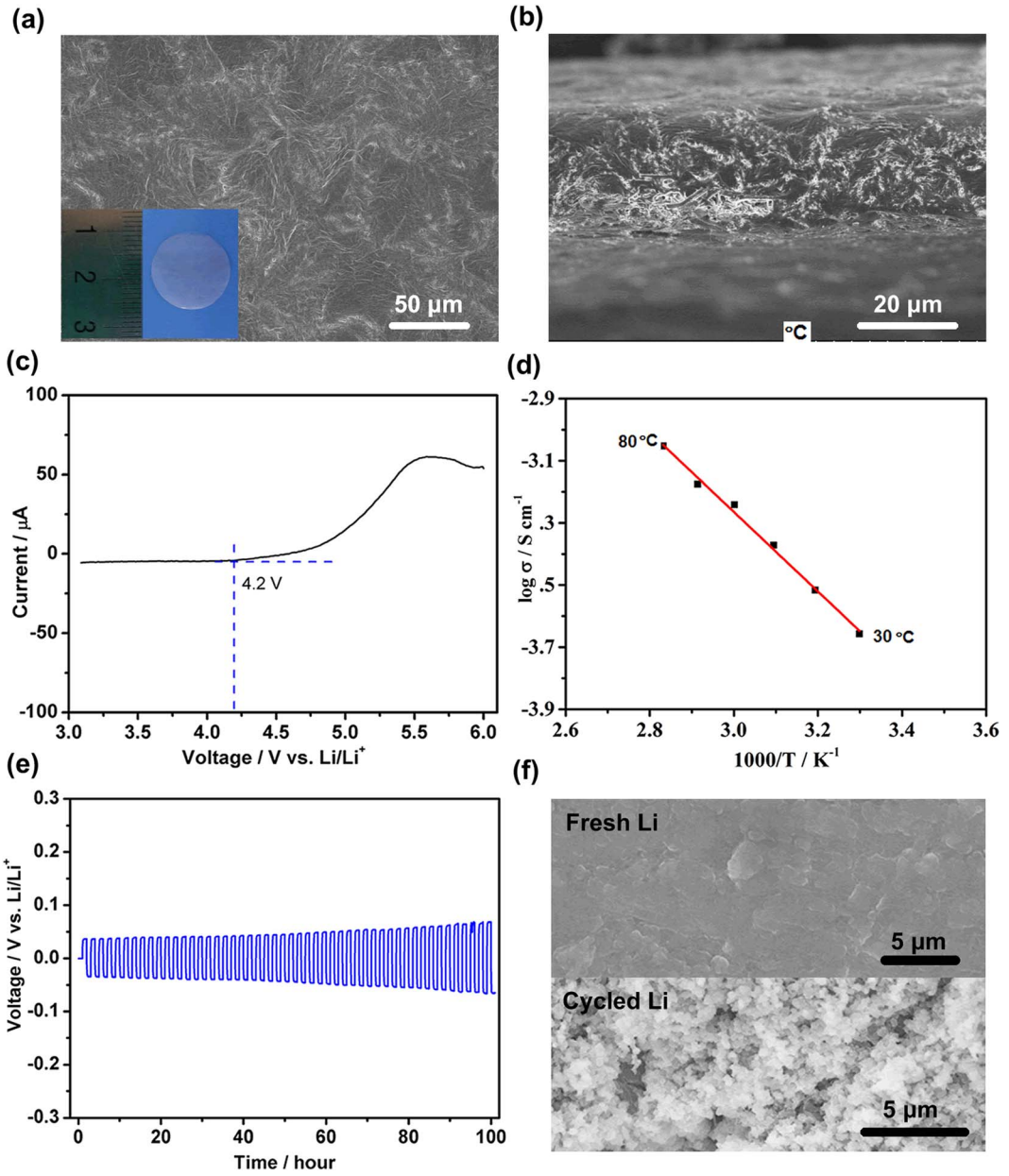

Figure 4. Typical SEM images of (a) surface and (b) cross section of cellulose-supported PEO-LiDFOB electrolyte. Inset was the photograph of PEO-LiDFOB electrolyte. (c) Linear sweep voltammetry curve of Li/PEO-LiDFOB/SS coin cell at 80°C. (d) Ionic conductivity of PEO-LiDFOB electrolyte from 30°C to 80°C. (e) Constant current (0.2 mA/cm^2) polarization curves of symmetric Li/PEO-LiDFOB/Li cell at 80°C. (f) Tpical SEM images of Li metal before and after cycling 100 hours in (e).

V vs. Li/Li$^+$, as shown in Figure S6. When the same $LiCoO_2$ cathode material was used in PEO-based all-solid-state LIBs, the electrochemical results indicated that the PECA-coated $LiCoO_2$ had higher discharge capacity, higher coulombic efficiency, and lower polarization than that of uncoated $LiCoO_2$ (Figure 5a). The initial discharge capacity for PECA-coated $LiCoO_2$ was 172.8 mAh/g, while that for bared $LiCoO_2$ was 144.5 mAh/g. Moreover, the capacity retention of PECA-coated $LiCoO_2$/PEO/Li cell was much better than the corresponding uncoated-$LiCoO_2$ cell (Figure 5b). To explore the reason of capacity fading in $LiCoO_2$/PEO-LiDFOB/Li cell and how PECA coating layer improved its electrochemical performance from the aspect of cathode/electrolyte interface, EIS of $LiCoO_2$/PEO-LiDFOB/Li and PECA-coated $LiCoO_2$/PEO-LiDFOB/Li cells at different cycle states were carried out. The results in Figures 5c–5d as well as Figure S7 and Table S1 showed the cycle number dependence of the impedance spectra for $LiCoO_2$/PEO-LiDFOB/Li and PECA-coated $LiCoO_2$/PEO-LiDFOB/Li cells, respectively. All the obtained plots were well fitted using the electric equivalent circuit shown in the inset of Figures 5c–5d. From the OCV state to the 20th discharge state, the bulk resistance (R_b) and interphase resistance (R_i) of $LiCoO_2$/PEO-LiDFOB/Li cell increased continuously. In a sharp contrast, the PECA-coated $LiCoO_2$/PEO-LiDFOB/Li cell showed less bulk and interphase resistance increase than that of $LiCoO_2$/PEO/Li cell from the OCV state to the 2nd discharge state. No obvious impedance increase was observed from the 2nd to the 20th discharge state. It indicated that the interface impedance of PECA-coated $LiCoO_2$/PEO-LiDFOB/Li cell was constant after two cycles charging and discharging. Furthermore, the R_b remained less than 10 Ω during cycling. Therefore, it can be concluded that the enhanced electrochemical performance of PECA-coated $LiCoO_2$/PEO-LiDFOB/Li in high voltage range was

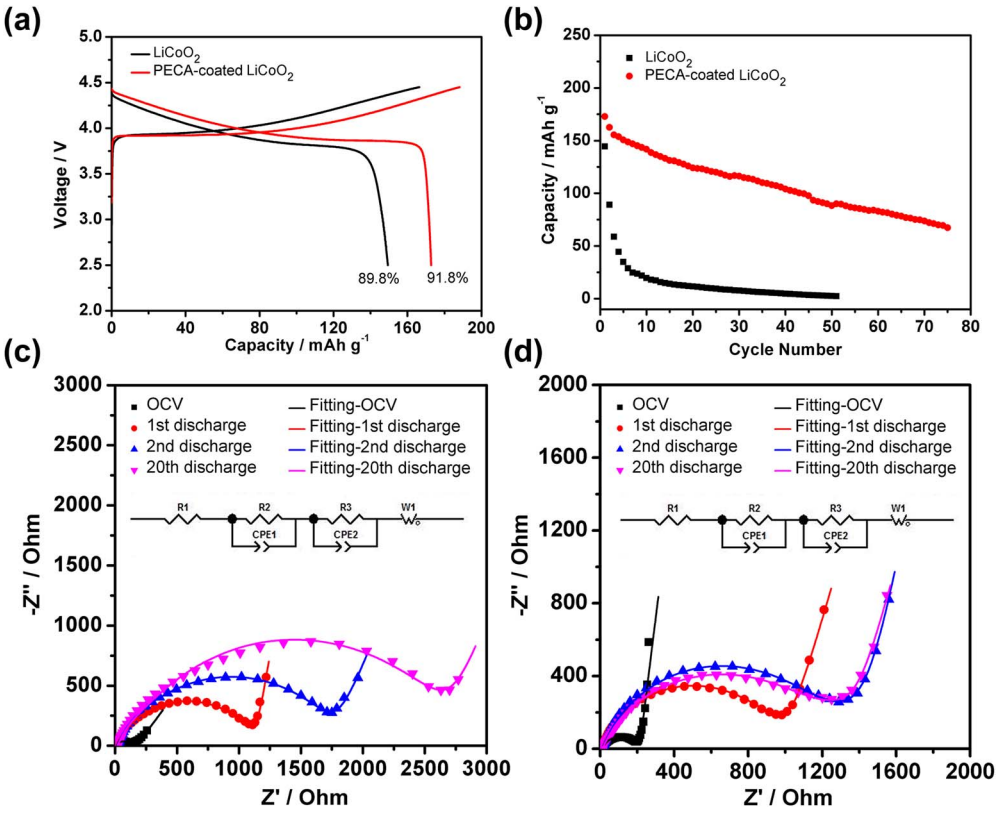

Figure 5. (a) The first cycle charge and discharge curves and (b) cycle performance of $LiCoO_2$/PEO-LiDFOB/Li and PECA-coated $LiCoO_2$/PEO-LiDFOB/Li cells at 80°C. Measured and simulated results of impedance plots for (c) $LiCoO_2$/PEO-LiDFOB/Li and (d) PECA-coated $LiCoO_2$/PEO-LiDFOB/Li cells at different cycle states. Insets are the corresponding electric equivalent circuits.

beneficial from the PECA coating layer on the surface of $LiCoO_2$, which can obviously suppress the interface impedance increase during cycling.

Investigation on the interface reaction.—To further explain the origin of the increased interphase impedance for $LiCoO_2$/PEO-LiDFOB/Li during cycling and the suppression effect of PECA coating layer on it, reflective FTIR spectra of $LiCoO_2$ cathode and PEO-LiDFOB electrolyte before and after 20 cycles were measured (Figure 6). Before FTIR measurement, the $LiCoO_2$ cathode and PEO-LiDFOB electrolyte were separated from each other manually. In the FTIR spectra of $LiCoO_2$ electrode and PEO-LiDFOB electrolyte withdrawn from the cycled $LiCoO_2$/PEO-LiDFOB/Li cell, the absorption peaks at 1794 and 1761 cm^{-1} disappeared, while the peak at 1721 cm^{-1} strengthened. According to the analyses of FTIR peak assignment in Figure S8 and Table S2, this result indicated the ring-opening reaction of $DFOB^-$ anion at high voltage.[28] Moreover, the absorption peaks between 1000 cm^{-1} and 1200 cm^{-1} split obviously in the cycled $LiCoO_2$/PEO-LiDFOB/Li cell, suggesting the weaken interaction between PEO and LiDFOB after battery cycling, which may be caused by the decomposition of LiDFOB.[29] On the contrary, the FTIR results of $LiCoO_2$ and PEO in the cycled PECA-coated $LiCoO_2$/PEO-LiDFOB/Li cell showed no obvious differences from that of the pristine PEO electrolyte. It means that the PECA coating

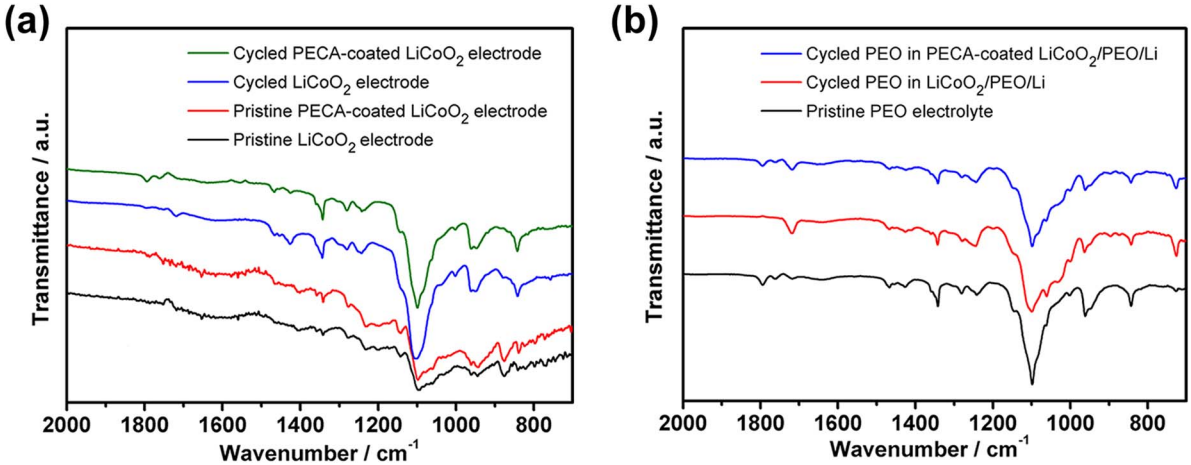

Figure 6. FTIR results of (a) $LiCoO_2$ electrode and (b) PEO electrolyte before and after charging/discharging 20 cycles.

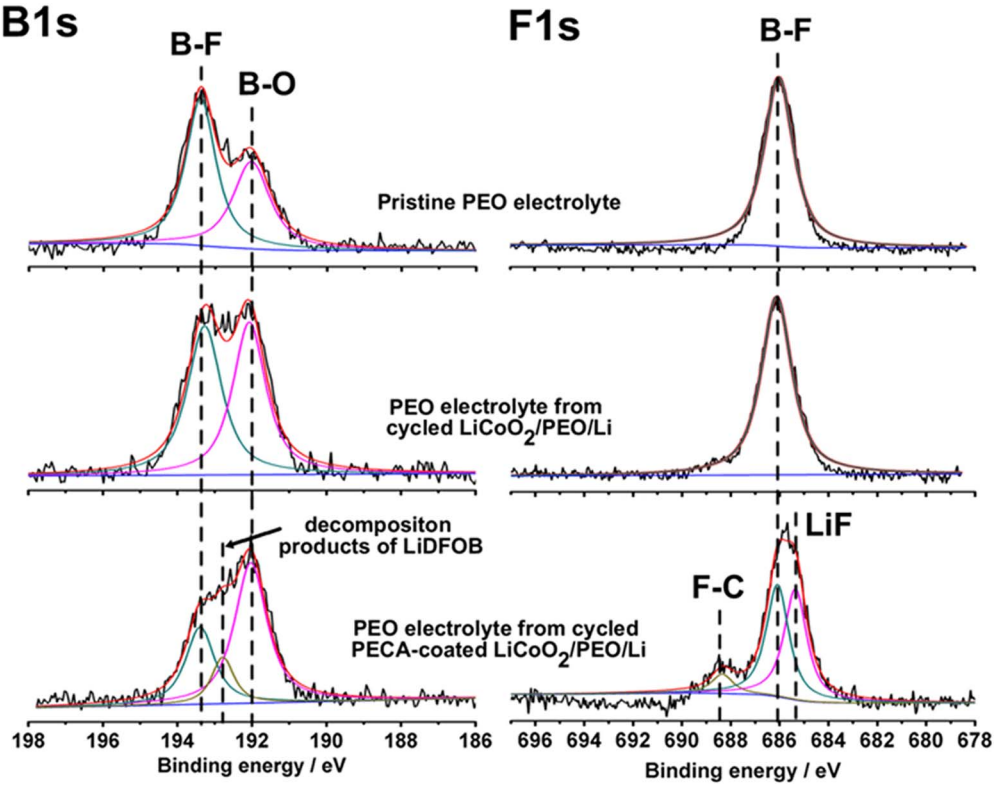

Figure 7. B1s and F1s XPS results of PEO electrolyte before and after charging/discharging 20 cycles.

can effectively suppress the ring-opening reaction of $DFOB^-$ anion at high voltage and guarantee the strong interaction between PEO and LiDFOB.

The decomposition of LiDFOB in $LiCoO_2$/PEO-LiDFOB/Li cell was also identified by the XPS results (Figure 7 and Figure S9). For the pristine PEO-LiDFOB electrolyte, the B1s peak at 192.0 eV, as well as the B1s peak at 193.4 eV and F1s peak at 686.1 eV, corresponded to B-O and B-F of LiDFOB, respectively.[30] After 20 cycles charging and discharging, the relative intensity of B-O peak increased remarkably, but the F1s (B-F) peak changed barely. Xu et al. have reported that the ring opening process could reduce the symmetry and the coordinated number of B center and make the B1s peak shift to a lower binding energy.[31] Thus, the increased relative intensity of B-O peak in PEO electrolyte from cycled $LiCoO_2$/PEO-LiDFOB/Li cell might be attributed to the ring opening process of LiDFOB.[30–32] As for PEO electrolyte from the PECA-coated $LiCoO_2$/PEO-LiDFOB/Li cell, the relative intensity of B-F decreased while that of the B-O peak heightened much more than that of the uncoated sample. It can be attributed to the LiF (F1s, 685.4 eV) and F-C (F1s, 688.3 eV) species on the surface of PEO electrolyte. Moreover, a new B1s peak emerged at 192.8 eV, which was associated with the decomposition products of LiDFOB, such as $Li_xBO_yF_z$ species.[30–33] Compared with the XPS results of PEO electrolyte from the $LiCoO_2$/PEO-LiDFOB/Li cell, these new species may be resulted from the interface reaction between LiDFOB and PECA.

According to the above analysis on FTIR and XPS results as well as the EIS results, it can be concluded that the compatibility between PEO-LiDFOB electrolyte and high voltage $LiCoO_2$ cathode was mainly influenced by the stability of Li salt LiDFOB instead of the PEO polymer. The PECA coating layer played an important role in enhancing the $LiCoO_2$/PEO-LiDFOB electrolyte interface stability. According to previous reports, LiDFOB was a general electrolyte additive in high voltage LIBs. Its $DFOB^-$ anions could oxidize to $F_2BOC\bullet O$ radical at 4.4 V vs. Li/Li^+, in which the boron strongly interacted with oxygen atoms in other molecules, such as carbonyl oxygen, ethers, and even bridging and nonbridging oxygens on the metal oxide surfaces.[28,34] As a result, $DFOB^-$ anions formed oxidation-resistant $(CO_2BF_2)_2$ dimers on the cathode surface, which was believed to suppress the decomposition of liquid electrolyte catalyzed by transition metals. However, in all-solid-state $LiCoO_2$/PEO/Li batteries, the ring-opening reaction of $DFOB^-$ anions by breaking B-F bond was observed, suggesting the oxidation decomposition products of LiDFOB in all-solid-state electrolyte were different from that in liquid electrolyte. Furthermore, the XPS results demonstrated that the $LiCoO_2$/PEO-LiDFOB electrolyte interface reactions were different from that of PECA-coated $LiCoO_2$/PEO-LiDFOB electrolyte. Therefore, the increased interface impedance in $LiCoO_2$/PEO/Li cell may be related with the interface decomposition of LiDFOB. The ring-opening reaction products of $DFOB^-$ anions at high voltage decreased the interaction between Li salt and PEO, which may lead to decreased Li^+ conductivity and increased the interface impedance. During battery cycling, the decomposition products of $DFOB^-$ anions seemed to be instable and then resulted in continually increased interface impedance. When PECA coating layer separated the $LiCoO_2$ and PEO electrolyte, only trace amounts of $DFOB^-$ anions decomposed into LiF and F-C compound in the first several cycles. As PECA was a Li^+ conductor, Li^+ transfer between $LiCoO_2$ and PEO electrolyte was fluently.[24] Therefore, the PECA coating was an effective way to suppress the interface impedance augment of $LiCoO_2$/PEO/Li cell by avoiding the continuous decomposition of LiDFOB and retaining the interaction between PEO and LiDFOB during high voltage cycling.

Conclusions

In conclusion, the interface stability between $LiCoO_2$ and PEO-LiDFOB electrolyte was challenged by high oxidation ability of $LiCoO_2$, the decomposition of LiDFOB, and the weak interaction between PEO and LiDFOB. As a result, the $LiCoO_2$/PEO-LiDFOB/Li cell showed continuous interface impedance increase and poor cycle performance. PECA coating on the surface of $LiCoO_2$ was an effective method to improve the interface stability between high voltage $LiCoO_2$ and PEO-LiDFOB electrolyte. The FTIR, XPS, and

electrochemical measurement results as well as the DFT calculation results indicated that the PECA coating decreased the oxidation ability of $LiCoO_2$, suppressed the decomposition of LiDFOB, and remained the interaction between PEO and LiDFOB during high voltage cycling. Thus, compared with the $LiCoO_2$/PEO-LiDFOB/Li cell, the PECA-coated $LiCoO_2$/PEO-LiDFOB/Li cell displayed decreased interface resistance and enhanced cycling stability during high voltage cycling. This work not only increases our understanding of interface stability between cathode and polymer electrolyte, but also proposes an effective method to modify the solid/solid interface in solid polymer LIBs. It will also inspire much further research on the interface issues of all-solid-state LIBs. Nevertheless, it is worth mentioning that the further identification of interface reaction products and the accurate interpretation of interface reaction mechanism are still challenged. The combination of ingenious battery design, advanced in-situ characterization method, and theoretical calculation are required for future interface research.

Acknowledgments

This work was financially supported by the funding from National Natural Science Foundation of China (No. 51502319), "135" Projects Fund of CAS-QIBEBT Director Innovation Foundation, the Strategic Priority Research Program of the Chinese Academy of Sciences (grant No. XDA09010105), the China Postdoctoral Science Foundation (2017M612366), the Think-Tank Mutual Fund of Qingdao Energy Storage Industry Scientific Research, the Qingdao Science and Technology Program (17-1-1-26-jch), and Qingdao Key Lab of Solar Energy Utilization & Energy Storage Technology. The authors declare no competing financial interest.

References

1. M. Armand, *Solid State Ionics*, **9–10**, 745 (1983).
2. F. Croce, G. B. Appetecchi, L. Persi, and B. Scrosati, *Nature*, **394**, 456 (1998).
3. L. Yue, J. Ma, J. Zhang, J. Zhao, S. Dong, Z. Liu, G. Cui, and L. Chen, *Energy Storage Materials*, **5**, 139 (2016).
4. A. Manthiram, X. Yu, and S. Wang, *Nature Reviews Materials*, **2**, 16103 (2017).
5. H. Zhang, C. Li, M. Piszcz, E. Coya, T. Rojo, L. M. Rodriguez-Martinez, M. Armand, and Z. Zhou, *Chem. Soc. Rev.*, **46**, 797 (2017).
6. A. C. Luntz, J. Voss, and K. Reuter, *J. Phys. Chem. Lett.*, **6**, 4599 (2015).
7. W. D. Richards, L. J. Miara, Y. Wang, J. C. Kim, and G. Ceder, *Chem. Mater.*, **28**, 266 (2016).
8. G. Pistoia, *Li-Ion Batteries-Advances and Application*, first ed, Elsevier, Oxford (2014).
9. S. Seki, Y. Kobayashi, H. Miyashiro, A. Yamanaka, Y. Mita, and T. Iwahori, *J. Power Sources*, **146**, 741 (2005).
10. S. Seki, Y. Kobayashi, H. Miyashiro, Y. Mita, and T. Iwahori, *Chem. Mater.*, **17**, 2041 (2005).
11. H. Miyashiro, Y. Kobayashi, S. Seki, Y. Mita, A. Usami, M. Nakayama, and M. Wakihara, *Chem. Mater.*, **17**, 5603 (2005).
12. Y. Kobayashi, S. Seki, M. Tabuchi, H. Miyashiro, Y. Mita, and T. Iwahori, *J. Electrochem. Soc.*, **152**, A1985 (2005).
13. Y. Kobayashi, S. Seki, A. Yamanaka, H. Miyashiro, Y. Mita, and T. Iwahori, *J. Power Sources*, **146**, 719 (2005).
14. Z. Liu, P. Hu, J. Ma, B. Qin, Z. Zhang, C. Mou, Y. Yao, and G. Cui, *Electrochim. Acta*, **236**, 221 (2017).
15. J. Zhang, L. Yue, P. Hu, Z. Liu, B. Qin, B. Zhang, Q. Wang, G. Ding, C. Zhang, X. Zhou, J. Yao, G. Cui, and L. Chen, *Sci. Rep.*, **4**, 6272 (2014).
16. J. P. Perdew, K. Burke, and M. Ernzerhof, *Phys. Rev. Lett.*, **77**, 3865 (1996).
17. G. Kresse and D. Joubert, *Phys. Rev. B*, **59**, 1758 (1999).
18. L. Hu, Z. Xiong, C. Ouyang, S. Shi, Y. Ji, M. Lei, Z. Wang, H. Li, X. Huang, and L. Chen, *Phys. Rev. B*, **71**, 125433 (2005).
19. F. Ning, S. Li, B. Xu, and C. Ouyang, *Solid State Ionics*, **263**, 46 (2014).
20. F. Xiong, H. Yan, Y. Chen, B. Xu, J. Le, and C. Ouyang, *Int. J. Electrochem. Sci.*, **7**, 9390 (2012).
21. L. A. Montoro, M. Abbate, and J. M. Rosolen, *Electrochem. Solid-State Lett.*, **3**, 410 (2000).
22. Y. Zhou, F. Bei, H. Ji, X. Yang, L. Lu, and X. Wang, *J. Mol. Struct.*, **737**, 117 (2005).
23. M. Han, S. Kim, and S. Liu, *Polym. Degrad. Stabil.*, **93**, 1243 (2008).
24. P. Hu, Y. Duan, D. Hu, B. Qin, J. Zhang, Q. Wang, Z. Liu, G. Cui, and L. Chen, *ACS Appl. Mater. Interfaces*, **7**, 4720 (2015).
25. H. G. M. Edwards and J. S. Day, *J. Raman Spectrosc.*, **35**, 555 (2004).
26. S. Verdier, L. El Ouatani, R. Dedryvere, F. Bonhomme, P. Biensan, and D. Gonbeau, *J. Electrochem. Soc.*, **154**, A1088 (2007).
27. J. Ma, Y. Gao, Z. Wang, and L. Chen, *J. Power Sources*, **258**, 314 (2014).
28. I. A. Shkrob, Y. Zhu, T. W. Marin, and D. P. Abraham, *J. Phys. Chem. C*, **117**, 23750 (2013).
29. A. R. Polu, D. K. Kim, and H. W. Rhee, *Ionics*, **21**, 2771 (2015).
30. M. Hu, J. Wei, L. Xing, and Z. Zhou, *J. Appl. Electrochem.*, **42**, 291 (2012).
31. K. Xu, U. Lee, S. Zhang, and T. R. Jow, *J. Electrochem. Soc.*, **151**, A2106 (2004).
32. M. Xu, L. Zhou, L. Hao, L. Xing, W. Li, and B. L. Lucht, *J. Power Sources*, **196**, 6794 (2011).
33. A. Xiao, L. Yang, B. L. Lucht, S. H. Kang, and D. P. Abraham, *J. Electrochem. Soc.*, **156**, A318 (2009).
34. Y. Zhu, Y. Li, M. Bettge, and D. P. Abraham, *J. Electrochem. Soc.*, **156**, A2109 (2012).